3-D quantitative dynamic contrast ultrasound for prostate cancer localization

Document license:
TAVERNE

DOI:
10.1016/j.ultrasmedbio.2017.12.005

Document status and date:
Published: 01/04/2018

Document Version:
Publisher's PDF, also known as Version of Record (includes final page, issue and volume numbers)

Please check the document version of this publication:

• A submitted manuscript is the version of the article upon submission and before peer-review. There can be important differences between the submitted version and the official published version of record. People interested in the research are advised to contact the author for the final version of the publication, or visit the DOI to the publisher's website.
• The final author version and the galley proof are versions of the publication after peer review.
• The final published version features the final layout of the paper including the volume, issue and page numbers.

Link to publication

Download date: 24. May. 2025

CrossMark

ELSEVIER

● *Original Contribution*

3-D QUANTITATIVE DYNAMIC CONTRAST ULTRASOUND FOR PROSTATE CANCER LOCALIZATION

STEFAN G. SCHALK,*,† JING HUANG,‡ JIA LI,‡ LIBERTARIO DEMI,* HESSEL WIJKSTRA,*,†
PINTONG HUANG,‡ and MASSIMO MISCHI*

* Department of Electrical Engineering, Eindhoven University of Technology, Eindhoven, The Netherlands; † Department of Urology, Academic Medical Center, Amsterdam, The Netherlands; and ‡ Department of Ultrasound, Second Affiliated Hospital of Zhejiang University School of Medicine, Hangzhou, China

Abstract—To investigate quantitative 3-D dynamic contrast-enhanced ultrasound (DCE-US) and, in particular 3-D contrast-ultrasound dispersion imaging (CUDI), for prostate cancer detection and localization, 43 patients referred for 10–12-core systematic biopsy underwent 3-D DCE-US. For each 3-D DCE-US recording, parametric maps of CUDI-based and perfusion-based parameters were computed. The parametric maps were divided in regions, each corresponding to a biopsy core. The obtained parameters were validated per biopsy location and after combining two or more adjacent regions. For CUDI by correlation (r) and for the wash-in time (WIT), a significant difference in parameter values between benign and malignant biopsy cores was found ($p < 0.001$). In a per-prostate analysis, sensitivity and specificity were 94% and 50% for r, and 53% and 81% for WIT. Based on these results, it can be concluded that quantitative 3-D DCE-US could aid in localizing prostate cancer. Therefore, we recommend follow-up studies to investigate its value for targeting biopsies. (E-mail: stefan.schalk@gmail.com)   © 2018 World Federation for Ultrasound in Medicine & Biology. All rights reserved.

Key Words: Contrast ultrasound, Dynamic contrast-enhanced ultrasound, 3-D ultrasound, Prostate cancer imaging, Dispersion imaging, Quantitative, Core needle biopsy, Systematic biopsy.

INTRODUCTION

The current standard method for prostate cancer (PCa) diagnosis is transrectal ultrasound (TRUS)-guided systematic biopsy, usually after suspicion has been raised by digital rectal examination (DRE) or an elevated serum prostate-specific antigen (PSA) level (Heidenreich et al. 2014). However, systematic biopsies frequently miss or undergrade tumors (Bjurlin et al. 2013; Kvåle et al. 2009). In the latest international guidelines, multiparametric magnetic resonance imaging (mpMRI) is recommended for patients with persistently elevated PSA level and a prior negative biopsy session (Barentsz et al. 2012; Heidenreich et al. 2014). However, MRI investigations cannot be performed at the bedside and are relatively costly. Several alternative TRUS-based techniques, such as (shear-wave) elastography, computer-aided TRUS and dynamic contrast-enhancedultrasound (DCE-US), have been developed and

they show promise for PCa detection (Sarkar and Das 2016).

In DCE-US, intravenously injected microbubbles with a size comparable to red blood cells are used as contrast agents. Although the resolution of DCE-US imaging is not in the range of the size of the microvasculature, the kinetics of the microbubbles through the microvasculature can be captured by recording their concentration over time. PCa growth requires angiogenic microvasculature, which has different structural properties (*e.g.,* increased tortuosity, presence of arteriovenous shunts, increased permeability) resulting in different microbubble kinetics (Russo et al. 2012). Therefore, several studies have been carried out using DCE-US imaging qualitatively to detect PCa (Halpern et al. 2012; Pallwein et al. 2008; Xie et al. 2012). DCE-US features related to PCa are rapid contrast enhancement, increased contrast enhancement and asymmetric flow patterns (Aigner et al. 2009; Seitz et al. 2011); however, their effects are usually very subtle and vanish within seconds. Consequently, interpretation of DCE-US recordings is rather subjective without technical aid. To increase objectivity and improve accuracy, the possibility

---

Address correspondence to: Stefan Schalk, Department of Electrical Engineering, Eindhoven University of Technology, Postbus 513, Flux 7.074, 5600 MB, Eindhoven, The Netherlands. E-mail: stefan.schalk@gmail.com

of using quantitative methods by extracting perfusion-based parameters from DCE-US recordings have been investigated (Cosgrove and Lassau 2010; Frinking et al. 2010; Smeenge et al. 2011). More recently, contrast-ultrasound dispersion imaging (CUDI) has been proposed as a novel approach to distinguish between angiogenic and healthy vasculature by focusing on contrast dispersion rather than on perfusion (Kuenen et al. 2011, 2013a, 2013b; Schalk et al. 2017). In fact, it was hypothesized that dispersion better reflects the underlying micro-vascular differences. At the origin of this technique, a model was fitted to acoustic time-intensity curves (TICs) in each pixel of a DCE-US recording (Kuenen et al. 2011). From the fit, a dispersion-related parameter could be extracted. Later it was shown that the similarity between neighboring TICs could be used as an indirect measure of local dispersion, which lead to better classification results (Kuenen et al. 2013a, 2013b; Schalk et al. 2017). Three similarity measures were investigated: temporal correlation (r), spectral coherence (ρ) and mutual information (I). However, the method was still limited by the 2-D nature of the recordings. Each plane required a separate injection of microbubbles, tumors between imaging planes were missed and out-of-plane flow could not be observed.

Using 3-D DCE-US enables imaging the vasculature in the entire prostate with a single injection of contrast agent and the inherently three-dimensional transport kinetics can be observed. In a recent study, the technical feasibility of 3-D CUDI as the first quantitative method using 3-D DCE-US for PCa was tested *in vivo* in two patients (Schalk et al. 2015b). Although the temporal resolution of 3-D DCE-US recordings was too low for model fitting, 3-D CUDI by similarity analysis was shown to be possible.

Because of the limitations discussed earlier, standard DCE-US is currently not recommended in the international guidelines as a routine PCa imaging technique (Heidenreich et al. 2014). However, advanced DCE-US methods may detect PCa more accurately and eventually play a role in PCa diagnosis. With its improved applicability, 3-D DCE-US may become a valuable diagnostic option, providing complementary information to DCE-MRI, which detects contrast extravascular leakage, or even represent a cost-effective alternative to mpMRI.

In this work, we tested the ability of quantitative 3-D DCE-US and, in particular 3-D CUDI by similarity analysis, for PCa detection by comparison with systematic biopsies in 43 patients. Three similarity and four perfusion parameters were extracted from the 3-D DCE-US recordings. We investigated which parameters could discriminate between benign and malignant tissue and made a preliminary estimation of their classification performance.

MATERIALS AND METHODS

Data collection

Between January 2015 and March 2016, 58 patients referred for systematic biopsy underwent 3-D DCE-US at the Second Affiliated Hospital of Zhejiang University (Hangzhou, Zhejiang, PR China). Inclusion criteria were age >18 y and referral for systematic biopsy and DCE-US based on elevated PSA level, abnormal DRE or lesions visible in MRI. This study was approved by the local institutional review board of the Second Affiliated Hospital of Zhejiang University. Written informed consent was obtained from all participants in the study in accordance with the World Medical Association Declaration of Helsinki.

After intravenous injection of 2.4 mL Sonovue (Bracco, Milan, Italy) microbubbles, 3-D DCE-US imaging was performed using a LOGIQ E9 ultrasound scanner (GE Healthcare, Wauwatosa, WI, USA) equipped with an RIC9-5 transducer. To maximize the volume rate, the imaging quality setting "BQ" was set to "low". The acoustic output power setting "AO%" was limited to "10" to prevent bubble disruption. More details on the data characteristics are reported in our technical feasibility study on 3-D CUDI (Schalk et al. 2015b). Each DCE-US recording lasted 2 min and was stored in raw Digital Imaging and Communications in Medicine format.

After technical evaluation of the DCE-US recordings, 13 patients were excluded (Fig. 1). In 7 of the 13 exclusions, the protocol was violated (wrong scanner
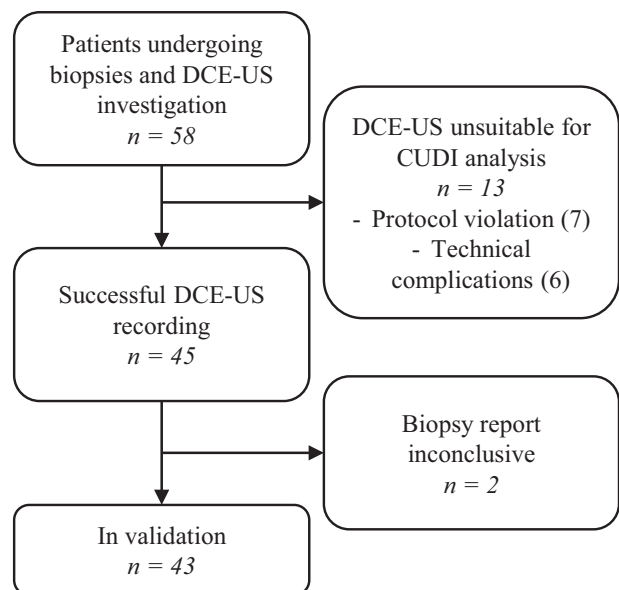

Fig. 1. Inclusion flowchart. Protocol violations included excessive probe movement, wrong scanner settings and untimely start of the recording. Technical complications encountered were low and inconsistent sample rate and lack of contrast signal. DCE-US = dynamic contrast-enhanced ultrasound; CUDI = contrast-ultrasound dispersion imaging.

settings, late start of the recording, strong probe movement). Five patients were excluded because of poor contrast enhancement or extremely slow wash-in (more than 30 s), which may be caused by an incorrect contrast injection. In one case, the 3-D DCE-US data had a very low, varying volume rate, most probably because of a problem with the data transfer or storage in the scanner. The remaining 45 valid recordings were prepared for analysis as previously proposed by Schalk et al. (2015b).

On each of these data sets, a CUDI similarity analysis as described by Schalk et al. (2015a; 2015b) was performed to generate parametric maps (Fig. 2) of *r*, *ρ* and I. To enable a fair comparison between the similarity measures, the same time window of 45 s, like the one described by Schalk et al. (2015b), was used for each measure. Additionally, several perfusion parameters proposed in the literature (Cosgrove and Lassau 2010) were extracted from the TICs at each voxel: wash-in time (WIT), peak intensity (PI), wash-in rate (WIR), and area under the TIC within the time window (AUC). A brief description of each of the parameters is given in Table 1.

Systematic biopsies were performed after a 12-core protocol in which 4 cores were taken from each of the basal, middle and apical part of the prostate. In 6 cases, 1 or 2 samples were not taken from the base or apex because of the small size of the prostate. For each biopsy location, the presence of malignancy and its corresponding Gleason score were reported. In 2 cases, the biopsy report was inconclusive; these patients were excluded from the study (Fig. 1). In summary, 43 cases were included and 15 were excluded for validation.

Validation

Comparison of the parametric maps with the biopsy results was done in a fine-to-coarse fashion, much like the validation carried out by Schalk et al. (2015b). First, the shape of the prostate was extracted from the DCE-US recordings by summing the DCE-US recordings over time and manually drawing the prostate contour in several planes along the three dimensions of the DCE-US recording. These contours were then interpolated using radial basis functions (Carr et al. 1997, 2001) to obtain a mask of the voxels inside the prostate. Next, the mask was divided in three regions by equidistant cuts along the basis-apex axis. Each region was again subdivided in four smaller regions by equidistant cuts along the right-left axis. The result is a division of the prostate mask into 12 regions (Fig. 3), each corresponding to a biopsy location.

To account for small inaccuracies in the prostate contour and movement in the DCE-US recording, a 5-mm erosion was applied to the boundaries of the prostate mask before analysis. In addition, 5-mm margins were applied between adjacent regions to prevent correlation between parameter values across these regions, caused by the
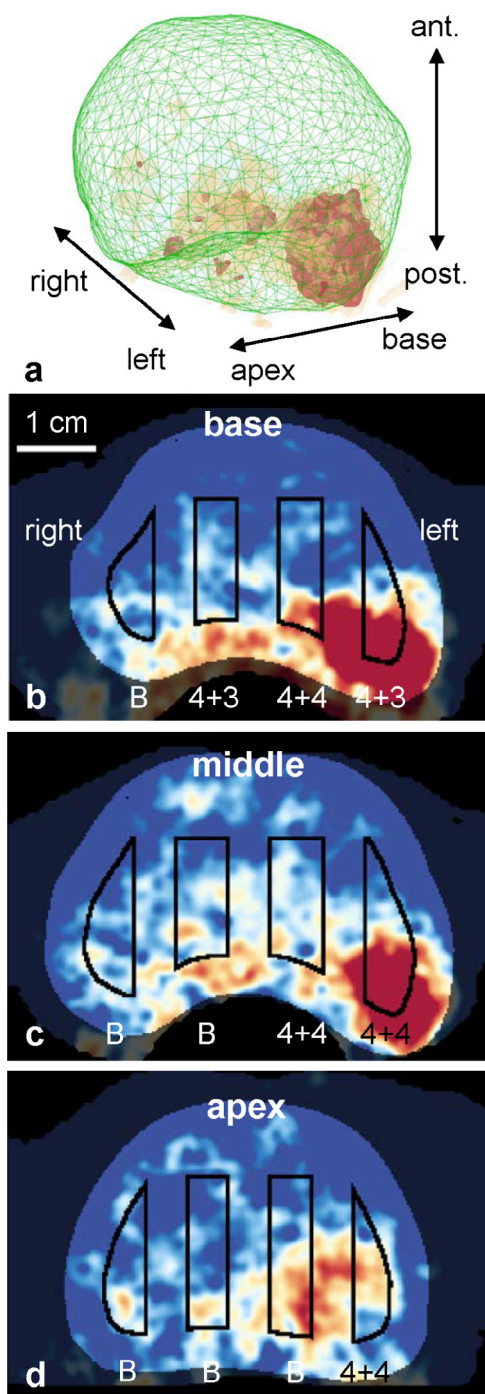
Fig. 2. Example of a parametric map of time-intensity curve (TIC) correlation (*r*). (a) 3-D parametric map. (b–d) transversal cross-sections at the base, middle and apex of the prostate. The 12 regions corresponding to the biopsy locations are shown (*black*). Gleason scores are written below each location (B = benign).

resolution of the parametric maps (Schalk et al. 2015b). Because the biopsy needle did not reach tissue deeper than 22 mm, only voxels up to 22 mm anterior to the tip of the transducer were considered for validation. Any region for

Table 1. Description of parameters obtained from 3-D DCE-US recordings

Parameter	Symbol	TH sign for mal	Description
Correlation	r	>	Cross-correlation between neighboring TICs.
Coherence	ρ	>	Cross-correlation between the frequency spectra of neighboring TICs.
Mutual information	I	>	Mutual information between neighboring TICs.
Wash-in time	WIT	<	Time between the appearance of microbubbles and the peak of a TIC.
Peak intensity	PI	>	Maximum linearized acoustic intensity in a TIC.
Wash-in rate	WIR	>	PI divided by WIT.
Area under the curve	AUC	>	Area under a linearized TIC within the applied 45-s time window.

TH = threshold; mal = malignancy; TIC = time-intensity curve.

which the biopsy report was inconclusive was excluded from further analysis.

The estimated DCE-US parameters were compared with the biopsy outcome in each region (test 1). A biopsy sample does not provide information on the size or shape of a tumor; as a result, a positive sample may also be caused by a small tumor (relative to the size of the region) or by a tumor that is only partly inside the region. In these cases, we do not expect the average parameter value in that region to be high, but do expect this parameter value to be high in a small percentage of the voxels in that region. For this reason, instead of the mean, the 90th percentile of each parameter value in a region was validated against biopsy outcome. For parameters for which malignancy was expected to result in lower values based on previous findings (Schalk et al. 2017), the 10th percentile was used. Additionally, since Gleason score is an important prognostic marker (Epstein et al. 2016), we tested parameters on their ability to differentiate between low grade (Gleason 6 and 7) and high grade (Gleason 8 to 10).

Because of the uncertainty in the location of the biopsy needle with respect to the regions, some biopsy samples may not have been taken in the region to which they were assigned, but in an adjacent region. To mitigate this effect, validation was repeated while combining adjacent regions, yielding 6, 3, 2 and 1 region(s) (Fig. 3) (test 2). A region was considered malignant if at least 1 biopsy sample within this region had a Gleason score ≥ 6. Differences among parameter values in benign and malignant regions were considered to be significant for $p < 0.05$, determined by

a Wilcoxon rank sum test. For each parameter, receiver operating characteristic (ROC) curves were generated. The area under the ROC curve was computed as a measure of classification performance.

In another test (test 3), the described validation was repeated on the divisions in 3, 2 and 1 regions. However, this time, a region was considered malignant if at least half of the biopsy cores were malignant and benign if all biopsy cores in it were benign. As a result, the parameters were tested for detection of larger cancerous areas. For parameters able to identify PCa, the differences between benign and malignant regions were expected to grow, resulting in a larger area under the ROC curve.

A last test (test 4) was designed to estimate the sensitivity and specificity of the best-performing parameters. In this test, each biopsy location was classified as positive or negative on the basis of the procedure used in test 1. However, because the chance of a biopsy core missing a tumor is relatively large, validation was performed in a left/right and per-prostate analysis (i.e., dividing prostates in 2 and 1 region[s]). A region was considered benign if all biopsy cores in this region were benign; it was considered malignant if at least one core was malignant. Nonetheless, if all cores in a systematic biopsy are negative, a significant chance remains that a tumor has been missed (Bjurlin et al. 2013). For this reason, we marked a false positive (FP) as "undecided" if less than 20% of the biopsy locations in a benign region were classified as malignant (i.e., 1 biopsy location for half and 2 for full prostates). Classification thresholds for the parameters were set to maximize Youden's index (Youden 1950).

RESULTS

Patients and biopsy characteristics are summarized in Table 2. In 17 out of 43 patients (40.0%), at least one of the biopsy cores contained malignant tissue. The median PSA level was higher for patients in which malignancy was found (13.8 ng/mL) than for patients without malignancy (7.6 ng/mL), although not significantly ($p = 0.21$). Malignancy was reported in 76 out of 507 biopsy cores (15.0%). For one biopsy core, malignancy was reported, but the Gleason score was not specified.
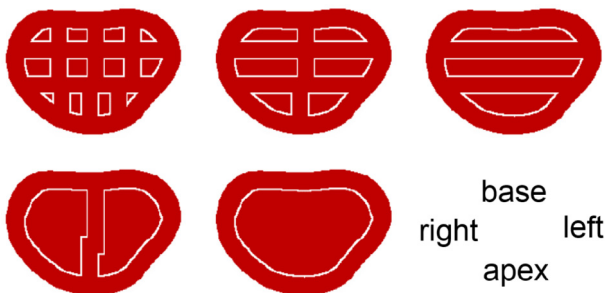

Fig. 3. Division of a prostate in 12, 6, 3, 2 and 1 region(s).

Table 2. Patient and biopsy characteristics

Mean (median; range) age [y]	69 (70; 47–81)
Mean (median; range) PSA [ng/mL]	23.1 (8.7; 0.3–340.0)
No malignant biopsy cores	9.8 (7.6; 1.4–21.0)
At least one malignant biopsy core	34.9 (13.8; 0.3–340.0)
Highest GS per biopsy [number of patients]	43
NC	26
GS unknown	1
3 + 3	3
3 + 4	3
4 + 3	5
3 + 5	1
4 + 4	1
5 + 3	0
4 + 5	0
5 + 4	2
5 + 5	1

GS = Gleason score; NC = no cancer.

Table 4. Areas under the ROC curves and *p*-values per parameter for test 3. In this analysis, malignant regions contain ≥50% malignant cores

	3 regions (21 mal; 95 ben)		2 regions (13 mal; 64 ben)		1 region (5 mal; 26 ben)	
	AUR	*p*	AUR	*p*	AUR	*p*
r	0.72*	<0.001	0.75*	<0.01	0.77*	0.032
ρ	0.60	0.082	0.60	0.13	0.56	0.34
I	0.57	0.14	0.62	0.095	0.58	0.29
WIT	0.69*	<0.01	0.66*	0.035	0.77*	0.032
PI	0.46	0.72	0.52	0.41	0.45	0.64
WIR	0.49	0.55	0.56	0.25	0.51	0.49
AUC	0.43	0.83	0.52	0.49	0.42	0.71

mal = malignant; ben = benign; AUR = area under ROC curve; r = correlation; ρ = coherence; I = mutual information; WIT = wash-in time; PI = peak intensity; WIR = wash-in rate; AUC = area under TIC curve.
* Statistically significant.

The area under the ROC curve (AUR) and *p*-value for each of the parameters tested in the fine-to-coarse validation (tests 1 and 2) are presented in Table 3. For each division, *r* resulted in the highest ROC curve area (0.57–0.67). Differences among benign and malignant regions were significant for all but one division. Also for ρ and *I*, a significant difference was found in one of the divisions. However, their AUR was much lower than that of *r*. The best-performing perfusion parameter was WIT with AURs between 0.54 and 0.64.

The results of the second fine-to-coarse analysis (test 3) are presented in Table 4. Only for *r* and WIT, a strong increase in AUR was observed. This result suggests that *r* and WIT are the parameters most suitable for discrimination between benign and malignant tissue.

Figure 4 depicts boxplots of the 90th percentile of *r* and 10th percentile of WIT for benign, low grade (Gleason 6 or 7), and high grade (Gleason 8–10) biopsy locations. For *r*, the mean ± standard deviations were 0.35 ± 0.09, 0.38 ± 0.08 and 0.41 ± 0.07, respectively. A significant increase in parameter values ($p < 0.01$) between benign and

low-grade biopsy locations was observed. The parameter *r* increased also for high-grade biopsy locations, but this increase was not significant ($p = 0.080$). A similar trend (but negative) was found for WIT, whose 10th percentile values for benign, low grade and high grade were 11.2 ± 2.2, 10.5 ± 2.3 and 8.4 ± 3.2, respectively. In this case, the difference between high grade and low grade was significant ($p < 0.01$), but that between benign and low grade was just insignificant ($p = 0.052$).

The confusion matrices of the left/right and perprostate analysis (test 4) for the two best performing parameters (*r* and WIT) are presented in Table 5. Regarding the left/right analysis, the sensitivity (Se.), specificity (Sp.), positive predictive value (PPV) and negative predictive value (NPV) for *r* were 65%, 80%, 58% and 84%, respectively. In the per-prostate analysis these values were 94%, 50%, 59% and 92%. Only 1 tumor, with Gleason score 4 + 3, was missed in this analysis. For WIT, the Se., Sp., PPV and NPV were 57%, 77%, 50% and 81% in the left/right analysis and 53%, 81%, 69% and 68% in the

Table 3. Areas under ROC curves and *p*-values per parameter for test 1 and 2. In these tests, malignant regions contain at least 1 malignant biopsy core

	12 regions (77 mal; 431 ben)		6 regions (50 mal; 211 ben)		3 regions (36 mal; 95 be.)		2 regions (23 mal; 64 ben)		1 region (17 mal; 26 ben)	
	AUR	*p*	AUR	*p*	AUR	*p*	AUR	*p*	AUR	*p*
r	0.65*	<0.001	0.64*	<0.001	0.65*	<0.01	0.67*	<0.01	0.57	0.22
ρ	0.56*	0.045	0.57	0.059	0.58	0.080	0.58	0.14	0.52	0.44
I	0.52	0.29	0.53	0.25	0.59	0.061	0.63*	0.036	0.52	0.41
WIT	0.64*	<0.001	0.62*	<0.01	0.59	0.055	0.59	0.096	0.54	0.35
PI	0.51	0.40	0.50	0.50	0.50	0.53	0.50	0.52	0.39	0.88
WIR	0.54	0.12	0.53	0.21	0.51	0.41	0.52	0.37	0.41	0.83
AUC	0.49	0.65	0.49	0.62	0.48	0.63	0.50	0.51	0.40	0.85

mal = malignant; ben = benign; AUR = area under ROC curve; *r* = correlation; ρ = coherence; *I* = mutual information; WIT = wash-in time; PI = peak intensity; WIR = wash-in rate; AUC = area under TIC curve.
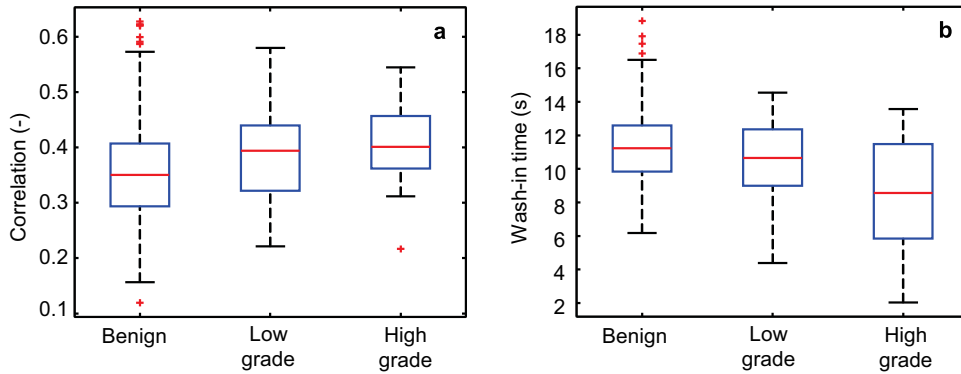* Statistically significant.

Fig. 4. Results grouped by Gleason grade. (a) Boxplots of the 90th percentile values within biopsy locations for correlation and (b) wash-in time. Outliers (indicated by *plus signs*) are defined as points ≥1.5 *w* away from the 25%–75% box with *w* equal to the box size.

per-prostate analysis. Using WIT, tumors were missed in 8 prostates. Their Gleason scores were 3 + 3 (2), 3 + 4 (1), 4 + 3 (3), 3 + 5 (1) and 5 + 4 (1).

DISCUSSION

In this study, we investigated whether and which 3-D DCE-US parameters could distinguish between benign and malignant prostate tissue. Both *r* and WIT showed a significant difference among locations corresponding to benign and malignant cores. In the left/right and per-prostate analyses, *r* resulted in a high Se. with acceptable Sp. from a clinical perspective. However, especially the high NPVs of 84% and 92%, respectively, are clinically interesting, as these results may exclude the possibility of the presence of cancer before biopsies have been taken. While *r* generally shows a higher Se. and NPV, WIT shows a higher Sp. and PPV. Combining the two in a multiparametric approach could exploit the benefit of both parameters. Moreover, strong indications were found of a relation between Gleason grade and parameter values of *r* and WIT, which could potentially improve risk stratification.

In a recent study by Postema et al. (2016), probability maps based on WIR statistics of 2-D DCE-US were

compared with systematic biopsy. On a per-prostate basis, an Se. of 73% and an Sp. of 58% were reported. These values are in between the Se. and Sp. achieved by *r* and WIT in the present study. Xie et al. (2012) used qualitative 2-D DCE-US to target cores in a 10-core biopsy to suspicious areas in 150 patients. The resulting Se. and Sp. stratified per patient were 86% and 56%, respectively. Our study shows that *r* can achieve comparable Se. and Sp. using 3-D DCE-US. Comparison of the performance of 3-D DCE-US with that of mpMRI is difficult because of the large range in Se. (68%–94%) and Sp. (21%–70%) reported in studies involving biopsy naive patients (Ahmed et al. 2017; Haider et al. 2016). We recommend performing a study that applies the two techniques in the same patient group to evaluate the differences.

Currently, the CUDI analysis takes a few hours to complete. However, the current implementation has not yet been optimized with respect to execution time and it runs on a single central processing unit. Because the analysis is performed locally using a shifting kernel, it is highly suitable for parallel computation. This may significantly reduce the execution time to just minutes. Compared with mpMRI, requiring a separate diagnostic session and complex multimodal fusion to perform biopsy targeting, CUDI enables performing diagnostic imaging and biopsy targeting in the same session with the same ultrasound system, strongly favoring the clinical workflow. Registration of the obtained parametric map with real-time ultrasound imaging is still necessary, but performed within the same imaging modality.

The validation methods applied in this study are subject to some limitations. First, the value of systematic biopsy as a ground truth is limited. There is a considerable chance that lesions are missed, decreasing the amount of FNs and TPs, while increasing the amount of FPs and TNs. Although we compensated somewhat for this effect in the last validation by ignoring FPs for which

Table 5. Confusion matrix of left/right and per-prostate cancer detection (test 4) for correlation (r) and wash-in time (WIT)

| | Left/right | | | | Per-prostate | | | |
| | Correlation | | Wash-in time | | Correlation | | Wash-in time | |
	Pos	Neg	Pos	Neg	Pos	Neg	Pos	Neg
Malignant	15	8	11	12	16	1	9	8
Benign	11	43	7	49	11	11	4	17
Undecided	9		7		4		5	

Pos = positive; Neg = negative.

less than 20% of the biopsy locations were classified as positive, the number of FNs, TPs and TNs remains biased. Therefore, the Se., Sp., PPV and NPV computed from test 4 should be interpreted as indications of the classification performance and further evaluated in future studies including radical prostatectomy specimens. The added value of using 3-D quantitative DCE-US in PCa diagnostics could be verified by a future study in which lesions are biopsied based on the parametric maps.

Moreover, AURs in the per-biopsy analysis have probably been underestimated for parameters able to differentiate between benign and malignant locations. Second, because biopsy was guided by free-hand TRUS, the estimated location of a biopsy core did not necessarily match its true location. For example, in the parametric map presented in Figure 2, the tumor was detected, but not all biopsy outcomes matched the parameter values at their estimated locations individually. The possible misalignment between true and estimated location complicated the comparison of single cores and was the primary reason to combine multiple cores. However, the AURs did not increase for larger regions. We may hypothesize that small tumors did not have enough influence on the parameter values in a large region. Moreover, when tumors had been missed by biopsy in an all-negative region, the parameter values in that region are not expected to be different from those with one or two positive cores. After tightening the definition of malignant regions to have malignancy in at least half of the cores, the AUR for r and WIT increased. This performance increase indicates that these parameters are actually influenced by the presence of PCa.

A standard reference for PCa studies is histopathology after radical prostatectomy. Although this ground truth is more reliable than the provided biopsy results, the population represented in those studies is strongly biased toward malignancy. The population represented in the biopsy data in this study reflects exactly the population targeted by quantitative 3-D DCE-US as a diagnostic tool. Comparison with radical prostatectomy could, however, be advantageous to evaluate the ability of the technique to estimate tumor size and shape, also at anterior sites, and to determine how many and which tumors are missed.

In the present study, parameter values have been directly compared with biopsy outcome. The learning curve and inter-observer variability present in clinical practice have not yet been accounted for and should be investigated in future studies. Such aspects could be tested in a clinical study comparing systematic biopsy and 3-D DCE-US targeted biopsy for prostate cancer detection.

In conclusion, quantitative analysis of 3-D DCE-US can be used to distinguish between benign and malignant tissue. For wash-in time and CUDI by TIC correlation, a relation between parameter value and biopsy outcome was proven. In addition, their parameter values seem to be related to Gleason grade, although further studies are required to confirm this finding. We recommend future investigation of quantitative 3-D DCE-US for guidance of targeted biopsies as a possible alternative or addition to mpMRI.

REFERENCES

Ahmed HU, El-Shater Bosaily A, Brown LC, Gabe R, Kaplan R, Parmar MK, Collaco-Moraes Y, Ward K, Hindley RG, Freeman A, Kirkham AP, Oldroyd R, Parker C, Emberton M, PROMIS Study Group. Diagnostic accuracy of multi-parametric MRI and TRUS biopsy in prostate cancer (PROMIS): A paired validating confirmatory study. Lancet 2017;389:815–822.

Aigner F, Pallwein L, Mitterberger M, Pinggera GM, Mikuz G, Horninger W, Frauscher F. Contrast-enhanced ultrasonography using cadence-contrast pulse sequencing technology for targeted biopsy of the prostate. BJU Int 2009;103:458–463.

Barentsz JO, Richenberg J, Clements R, Choyke P, Verma S, Villeirs G, Rouviere O, Logager V, Fütterer JJ, European Society of Urogenital Radiology. ESUR prostate MR guidelines 2012. Eur Radiol 2012;22:746–757.

Bjurlin MA, Carter HB, Schellhammer P, Cookson MS, Gomella LG, Troyer D, Wheeler TM, Schlossberg S, Penson DF, Taneja SS. Optimization of initial prostate biopsy in clinical practice: Sampling, labeling and specimen processing. J Urol 2013;189:2039–2046.

Carr JC, Fright WR, Beatson RK. Surface interpolation with radial basis functions for medical imaging. IEEE Trans Med Imaging 1997;16:96–107.

Carr JC, Beatson RK, Cherrie JB, Mitchell TJ, Fright WR, McCallum BC, Evans TR. Reconstruction and representation of 3D objects with radial basis functions. In: SIGGRAPH '01 Proceedings of the 28th annual conference on computer graphics and interactive techniques. New York, NY: ACM; 2001. p. 67–76.

Cosgrove D, Lassau N. Imaging of perfusion using ultrasound. Eur J Nucl Med Mol Imaging 2010;37(Suppl 1):S65–S85.

Epstein JI, Egevad L, Amin MB, Delahunt B, Srigley JR, Humphrey PA. The 2014 International Society of Urological Pathology (ISUP) Consensus Conference on Gleason Grading of Prostatic Carcinoma: Definition of grading patterns and proposal for a new grading system. Am J Surg Pathol 2016;40:244–252.

Frinking PJA, Mercier L, Rognin N, Arditi M, Tranquart F, Schneider M. Real-time contrast-enhanced ultrasound parametric imaging in prostate. In: Proceedings of the 15th European symposium on ultrasound contrast imaging. Rotterdam, The Netherlands: ICUS; 2010. p. 40–49.

Haider MA, Yao X, Loblaw A, Finelli A. Multiparametric magnetic resonance imaging in the diagnosis of prostate cancer: A systematic review. Clin Oncol (R Coll Radiol) 2016;28:550–567.

Halpern EJ, Gomella LG, Forsberg F, McCue PA, Trabulsi EJ. Contrast enhanced transrectal ultrasound for the detection of prostate cancer: A randomized, double-blind trial of dutasteride pretreatment. J Urol 2012;188:1739–1745.

Heidenreich A, Bastian PJ, Bellmunt J, Bolla M, Joniau S, van der Kwast T, Mason M, Matveev V, Wiegel T, Zattoni F, Mottet N. EAU Guidelines on prostate cancer. Part 1: Screening, diagnosis, and local treatment with curative intent—Update 2013. Eur Urol 2014;65:124–137.

Kuenen MPJ, Mischi M, Wijkstra H. Contrast-ultrasound diffusion imaging for localization of prostate cancer. IEEE Trans Med Imaging 2011;30:1493–1502.

Kuenen MPJ, Saidov TA, Wijkstra H, De la Rosette JJMCH, Mischi M. Spatiotemporal correlation of ultrasound contrast agent dilution curves for angiogenesis localization by dispersion imaging. IEEE Trans Ultrason Ferroelectr Freq Control 2013a;60:2665–2669.

Kuenen MPJ, Saidov TA, Wijkstra H, Mischi M. Contrast-ultrasound dispersion imaging for prostate cancer localization by improved spatiotemporal similarity analysis. Ultrasound Med Biol 2013b;39: 1631–1641.

Kvåle R, Møller B, Wahlqvist R, Fosså SD, Berner A, Busch C, Kyrdalen AE, Svindland A, Viset T, Halvorsen OJ. Concordance between Gleason scores of needle biopsies and radical prostatectomy specimens: A population-based study. BJU Int 2009;103:1647– 1654.

Pallwein L, Mitterberger M, Pelzer A, Bartsch G, Strasser H, Pinggera GM, Aigner F, Gradl J, zur Nedden D, Frauscher F. Ultrasound of prostate cancer: Recent advances. Eur Radiol 2008;18:707–715.

Postema AW, Frinking PJA, Smeenge M, De Reijke TM, De la Rosette JJ, Tranquart F, Wijkstra H. Dynamic contrast-enhanced ultrasound parametric imaging for the detection of prostate cancer. BJU Int 2016;117:598–603.

Russo G, Mischi M, Scheepens W, De la Rosette JJMCH, Wijkstra H. Angiogenesis in prostate cancer: Onset, progression and imaging. BJU Int 2012;110:E794–E808.

Sarkar S, Das S. A review of imaging methods for prostate cancer detection. Biomed Eng Comput Biol 2016;7(Suppl 1):1–15.

Schalk S, Demi L, Bouhouch N, Kuenen M, Postema A, De la Rosette J, Wijkstra H, Tjalkens T, Mischi M. Contrast-enhanced ultrasound angiogenesis imaging by mutual information analysis for prostate cancer localization. IEEE Trans Biomed Eng 2017;64:661– 670.

Schalk SG, Demi L, Smeenge M, De la Rosette JJ, Huang P, Wijkstra H, Mischi M. 3D contrast ultrasound dispersion imaging by mutual information for prostate cancer localization. In: IEEE Int Ultrason Symp 2015a;1–4.

Schalk SG, Demi L, Smeenge M, Mills DM, Wallace KD, De la Rosette JJ, Wijkstra H, Mischi M. 4-D spatiotemporal analysis of ultrasound contrast agent dispersion for prostate cancer localization: A feasibility study. IEEE Trans Ultrason Ferroelectr Freq Control 2015b;62:839–851.

Seitz M, Gratzke C, Schlenker B, Buchner A, Karl A, Roosen A, Singer BB, Bastian PJ, Ergün S, Stief CG, Reich O, Tilki D. Contrast-enhanced transrectal ultrasound (CE-TRUS) with cadence-contrast pulse sequence (CPS) technology for the identification of prostate cancer. Urol Oncol 2011;29:295–301.

Smeenge M, Mischi M, Laguna Pes MP, De la Rosette JJ, Wijkstra H. Novel contrast-enhanced ultrasound imaging in prostate cancer. World J Urol 2011;29:581–587.

Xie SW, Li HL, Du J, Xia JG, Guo YF, Xin M, Li FH. Contrast-enhanced ultrasonography with contrast-tuned imaging technology for the detection of prostate cancer: Comparison with conventional ultrasonography. BJU Int 2012;109:1620–1626.

Youden WJ. Index for rating diagnostic tests. Cancer 1950;3:32– 35.